THE JOURNAL OF PHYSICAL CHEMISTRY C

Article

pubs.acs.org/JPCC

Effect of Silver Nanoparticles on the Photophysics of Riboflavin: Consequences on the ROS Generation

María Belén Rivas Aiello,[†] Juan José Romero,[†] Sonia G. Bertolotti,[‡] Mónica C. Gonzalez,[†] and Daniel O. Mártire*[,†]

[†]Instituto de Investigaciones Fisicoquímicas Teóricas y Aplicadas (INIFTA), Facultad de Ciencias Exactas, Universidad Nacional de La Plata, C. C. 16, Suc. 4, 1900 La Plata, Argentina

[‡]Departamento de Química, Universidad Nacional de Río Cuarto, 5800 Río Cuarto, Argentina

Supporting Information

ABSTRACT: Metal-enhanced singlet oxygen, $O_2(^1\Delta_g)$, generation is a desirable effect to augment the amount of $O_2(^1\Delta_g)$ produced upon irradiation of organic sensitizers. Herein, we employed pectin for stabilizing 9 nm silver nanoparticles and showed that these particles are able to form a ground-sate complex with riboflavin (Rf). Pump−probe transient absorption spectroscopy and laser flash-photolysis experiments proved that the excited state of the riboflavin−Ag complex feeds the triplet state of the sensitizer, which results in an enhanced intersystem crossing process. The higher amounts of riboflavin triplet states formed in the presence of the nanoparticles result in higher yields of singlet oxygen and hydrogen peroxide produced in the irradiated colloidal suspensions. As a result, not only the effect on singlet oxygen but also the effect on superoxide radical ion should contribute to a better performance of Riboflavin as a sensitizer applied to the photodynamic therapy of tumors.

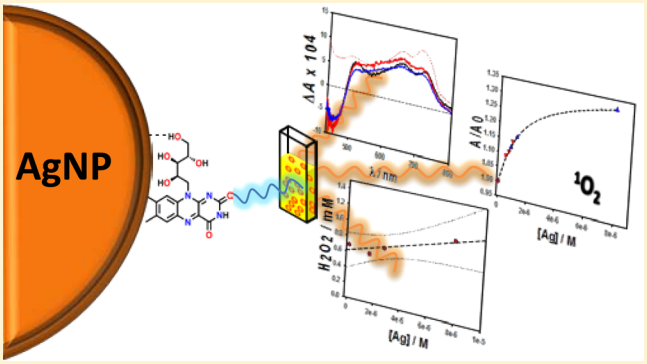

INTRODUCTION

Singlet oxygen, $O_2(^1\Delta_g)$, is the lowest excited state of molecular oxygen.[1−3] The treatment procedure named photodynamic therapy (PDT) is based on the production of $O_2(^1\Delta_g)$ for the eradication of diseased tissue.[4]

Singlet oxygen is most commonly and conveniently produced via photosensitization. Upon light absorption sensitizers produce a triplet state, which is quenched by the ground state of molecular oxygen in a collision-dependent process to yield singlet oxygen.[2,5]

The inefficient production of $O_2(^1\Delta_g)$ can restrict the use of PDT photosensitizers. Metal-enhanced $O_2(^1\Delta_g)$ generation is a desirable effect to augment the amount of $O_2(^1\Delta_g)$ produced.[6]

Light excitation of coherent oscillation of the free electrons in metallic nanoparticles produces localized surface plasmon resonance (LSPR).[7] In addition to the electromagnetic field enhancement, coupling of surface plasmons to molecular electronic transitions can take place.[8] The LSPR can also very much affect the excited states of the molecules for instance through energy or charge transfer processes.[8,9]

Riboflavin (Rf), the water-soluble vitamin B2, is the prosthetic group in flavine oxidoreductase enzymes and is an efficient photosensitizer.[10] Upon irradiation the one-electron transfer from donors to the lowest excited state of Rf, $^3Rf^*$, is called the Type I mechanism, which initiates free radical processes. Energy-transfer from $^3Rf^*$ to ground state oxygen leads to formation of $O_2(^1\Delta_g)$ with a quantum yield of 0.54 and is responsible for the oxidation of substrates through a Type II mechanism.[11−13]

Recently, using Rf as the sensitizer, the enhancement of $O_2(^1\Delta_g)$ generation by pectin-coated silver nanoparticles (Pec·AgNP) was demonstrated by an indirect method employing the fluorescent sensor green reagent.[14] These authors also reported an increase of Rf fluorescence emission in the presence of the nanoparticles.

The aim of the present work is to investigate in depth the effect of Pec·AgNP on the photophysics of Rf by employing a battery of spectroscopic techniques: steady-state fluorescence spectroscopy, time-correlated single-photon counting (TCSPC), pump−probe transient absorption spectroscopy, laser flash-photolysis, and time-resolved phosphorescence of singlet oxygen. To that purpose, a modification of the reported procedure[15] was employed to prepare Pec·AgNP. The nanoparticles were characterized by high-resolution transmission electron microscopy (HR-TEM), zeta potential, and UV−visible and infrared Fourier transform spectroscopy (FTIR) spectroscopies.

Received: June 24, 2016
Revised: August 31, 2016
Published: September 1, 2016

DOI: 10.1021/acs.jpcc.6b06385
J. Phys. Chem. C 2016, 120, 21967−21975

MATERIALS AND METHODS

Materials. Riboflavin and pectin from apple were purchased from Sigma-Aldrich. Silver nitrate was obtained from Biopack and sodium hydroxide from J. T. Baker. All experiments were performed with deionized water.

Synthesis of Pectin-Coated Silver Nanoparticles (Pec·AgNP). A modification of a literature method was employed.[15] In order to ensure complete solubilization an aqueous solution containing 10 g·L^{-1} of pectin was prepared by heating at ∼60 °C for about 45 min. After cooling at room temperature, aqueous 0.1 M $AgNO_3$ (1 mM final concentration) and NaOH solutions (final concentration 25 mM) were added rapidly under vigorous stirring for 6 h.

Characterization of Pec·AgNP. The particles size was measured by HR-TEM. The images were obtained with a CM200-FEG (Philips) instrument. The UV−visible extinction spectrum of the Pec·AgNP suspensions was measured with a T90+ PG spectrophotometer with an integrating sphere accessory.

In order to characterize the functional groups present in the nanoparticles, FTIR was performed on a Thermo Scientific Nicolet 380 FT-IR Spectrometer with an ATR sampling accessory Pike Miracle. Spectra between 550 and 4000 cm^{-1} were recorded for the solid samples with 1 cm^{-1} resolution.

The zeta potential measurements of 125 mg L^{-1} suspensions were carried out at 25.0 ± 0.1 °C with a Brookhaven 90Plus/Bi-MAS instrument, operating at λ = 635 nm from a 15 mW solid state laser.

The concentration of the nanoparticles calculated from the measured diameter and the metal density (10.5 g/cm^3)[16] is lower than the concentration of silver in the samples by a factor coincident with the average number of Ag atoms per particle $N_{Ag} = 2.2 \times 10^4$. From now on, the concentration of Ag will be specified.

Fluorescence Measurements. Fluorescence data were obtained with a HORIBA JOBIN-YVON Spex Fluorolog FL3-11. For the steady-state measurements the excitation wavelength was 355 nm. The Rf fluorescence spectra were coincident with reported data.[17] Luminescence lifetime measurements were performed with TCSPC using LED excitation at 388 nm operating at 1 MHz (fwhm ≈ 1.2 ns). The samples were diluted to avoid saturation of the emission detector.

Laser Flash-Photolysis with 355 nm Excitation. The excitation was the third harmonic (355 nm) of a Nd:YAG Spectron SL 400 laser (18 ns fwhm). The instrumentation has been described elsewhere.[18]

Pump−Probe and Laser Flash-Photolysis with 400 nm Excitation. The pump−probe measurements were performed using instrumentation that has been described previously.[19] The laser pulses of 100 fs at 800 nm were generated from an amplified, mode-locked titanium sapphire kilohertz laser system (Millennia/Tsunami/Spitfire, Spectra Physics). The instrument response function was ca. 150 fs. The polarization between pump and probe was set to the magic angle (54.7°). For the LFP experiments at 400 nm the same excitation setup was employed, and the detection portion of the spectrometer (EOS) was manufactured by Ultrafast Systems.

Since the spectra at short times show the contribution of several species, global analysis of the transient absorption data was performed. Here, we present both evolution-associated difference spectra (EADS) and decay-associated difference spectra (DADS). The analysis program calculates both EADS and DADS, and the time constants that follow from the analysis apply to both.[20] Random errors associated with the reported lifetimes were typically ≤5%.

Singlet Oxygen ($O_2(^1\Delta_g)$) Measurements. $O_2(^1\Delta_g)$ measurements were carried out using instrumentation that has been described previously[21] employing the excitation wavelength of 420 nm. For the experiments performed at λ^{exc} = 355 nm the third harmonic of a Nd:YAG Surelite II laser (7 ns fwhm and 14 mJ per pulse at 355 nm) (Continuum, San Jose, CA, USA) was employed as excitation source. The $O_2(^1\Delta_g)$ emission at 1270 nm was detected with an amplified Judson J 116/8sp germanium detector (5 mm diameter) (Teledyne Judson Technologies, Montgomeryville, PA).

The singlet oxygen experiments at λ^{exc} = 355 nm were performed in D_2O because the lifetime of $O_2(^1\Delta_g)$ in D_2O is longer than that in H_2O, which makes the phosphorescence measurement easier.[22] The absorbance of Rf samples with and without Pec·AgNP was adjusted to 0.50 at the excitation wavelength. The lifetimes measured in H_2O and D_2O were 3.3 and 68 μs, respectively, in very good agreement with reported data in these solvents.[22] Linear plots of the $O_2(^1\Delta_g)$ phosphorescence intensity vs incident laser fluence were obtained.

Procedure Employed for the Measurement of [H_2O_2]. Initial rates of H_2O_2 production (RH_2O_2) were measured in irradiated Rf solutions and dispersions of Pec·AgNP in Rf solutions. The excitation source was the third harmonic (355 nm) of the Nd:YAG Surelite II laser. H_2O_2 concentrations were measured employing a commercial kit from Wiener for cholesterol quantization.[23] Samples of 1 mL of the reaction mixture were mixed with 1 mL of the reagent. After 5 min of incubation at 37 °C the absorption spectra were measured.

RESULTS AND DISCUSSION

Characterization of Pec·AgNP. Figure S1a (see Supporting Information) shows HR-TEM images of the Pec·AgNP and the corresponding size distribution histogram. The calculated average particles diameter is 9 ± 2 nm.

The absorption maximum of the plasmon resonance band in aqueous suspensions of Pec-AgNP was 414 nm (see Figure S1b in the Supporting Information).

For underivatized Ag nanoparticles, the pH of zero charge is about 7.[24] Figure S1c (Supporting Information) shows the measured zeta potential values of aqueous suspensions of Pec·AgNP in the pH range 4−10. The negative zeta potential in the whole pH range further confirms the effective coating of the particles.

Figure S1d (Supporting Information) shows the comparison of the IR spectrum of the composite to that of pectin.[25] The spectra exhibit a broad band between 3600 and 2500 cm^{-1} due to hydroxyl stretching vibration, which can form inter- and intramolecular hydrogen bonds.[26] Bands around 2950 cm^{-1} (3000−2800 cm^{-1}) arise from asymmetrical stretching of C−H, CH_2, and CH_3 groups. In pectin samples, the C−H stretching vibrations appear as a band overlapped with the broader O−H band that ranges from 2500 to 3600 cm^{-1}. Stronger bands in the regions of 1760−1745 and 1640, 1620 cm^{-1} are assigned to the stretching vibrations of ester carbonyl (C═O) and carboxylate ion (COO^-), respectively.

Ground-State Interaction of Rf with Pec·AgNP. The concentrations of Rf and Pec·AgNP used in the photochemical experiments were chosen to ensure that the excitation light was

DOI: 10.1021/acs.jpcc.6b06385
J. Phys. Chem. C 2016, 120, 21967−21975

mainly absorbed by Rf, i.e., for all the experiments described below the absorption of Pec·AgNP at the excitation wavelength was at least 10 times lower than that of Rf. The possible ground-sate complexation of Ag with Rf under the conditions of the photochemical experiments was evaluated from the differences in the UV−vis spectrum of Rf in the presence of various amounts of Pec·AgNP.

The absorption spectra of an aqueous solution of 57 μM Rf in the presence of various amounts of Pec·AgNP shows an increase in absorbance indicating the association of Rf to colloidal silver (see Figure 1). The Rf···Pec·AgNP complex formation is given by reaction (1) in Scheme 1.

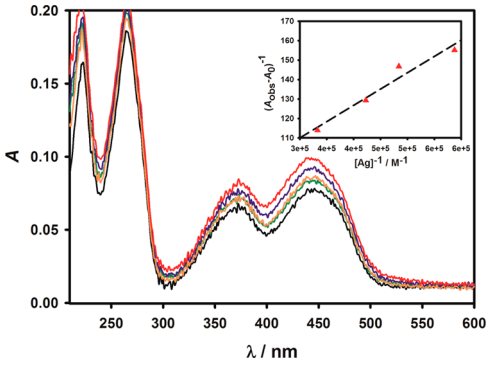

Figure 1. UV−visible absorption spectra of 57 μM Rf in the absence (black) and presence of various amounts of Pec·AgNP. The contribution of the Pec·AgNP in the mixtures was subtracted from the measured spectra by software. The silver concentrations are 7.88 μM (red), 1.57 μM (blue), 1.18 μM (orange), and 0.79 μM (green). Inset: Plot of $(\mathrm{Abs} - A_0)^{-1}$ vs $[\mathrm{Ag}]^{-1}$.

Scheme 1. Main Steps of the Proposed Reaction Mechanism in the Absence of Oxygen

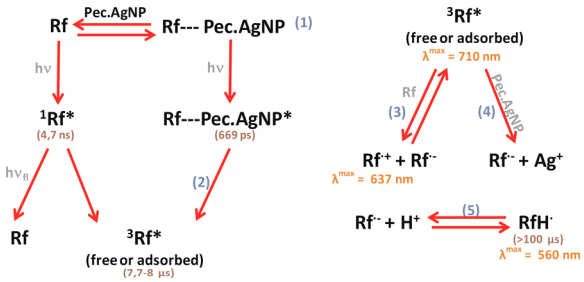

The apparent equilibrium constant K_{app} for the formation of the complex was determined according to the method reported by Benesi and Hildebrand (eq I).[27]

$$\frac{1}{A_{obs} - A_0} = \frac{1}{A_c - A_0} + \frac{1}{K_{app}(A_c - A_0)[Ag]} \qquad (I)$$

In eq I A_{obs} is the observed absorbance at 440 nm of Rf samples containing different concentrations of Pec·AgNP, and A_0 and A_c are the absorbances of Rf and the complex at 440 nm, respectively. The value of K_{app} obtained from the ratio of the intercept to the slope of the linear plot shown in the inset of Figure 1 is $(2.8 \pm 0.3) \times 10^4$ M^{-1}.

These data indicate that the amount of complexed Rf is ≤4% in the TCSPC experiments, ≤5% in the experiments with λ^{exc} = 400 nm, and ≤14% in the experiments with λ^{exc} = 355 nm.

Mokashi et al.[28] studied the complexation of Rf with citrate-stabilized silver nanoparticles and found from absorbance measurements an apparent binding constant of 1.5×10^3 M^{-1}. This fact and the coincidence of the absorption spectra of mixtures of pectin and Rf with the sum of the individual components (results not shown) support the interaction Rf with the silver atoms of Pec·AgNP.

Effect of Pec·AgNP on the Fluorescence of Rf. Within the Pec·AgNP concentration range employed for UV−visible absorption experiments, the fluorescence lifetime of Rf remained constant and equal to 4.7 ± 0.1 ns (see Table S1 of the Supporting Information), which rules out the occurrence of collision-dependent or FRET quenching processes. However, a modest quenching effect is observed in the steady-state experiments (see Figure S2 of the Supporting Information), in complete agreement with the TCSPC data if the ground-state complex is nonfluorescent.

Pump−Probe Experiments (λ^{exc} = 400 nm). In the case of metal nanoparticles, excitation of the electrons by a femtosecond laser pulse leads to a perturbation of the electron distribution in the metal. This electron distribution thermalizes through electron−electron scattering and then electron−phonon and phonon−phonon interactions are responsible for a complete relaxation of the initially absorbed photon energy.[29,30] In the case of nanoparticles, the difference spectrum shows the transient bleach centered at the plasmon resonance band maximum with two positive absorption bands at lower and higher wavelengths.[31]

All the experiments were performed under Ar-saturation. Figure 2a shows the EADS obtained for the blank experiments with Ag nanoparticles in the absence of Rf. For the two shorter decay times (0.32 and 3.93 ps) the lower energy wing is observed. The electron−electron scattering (typically on the order of 10 fs)[32] is not observed here because of the time resolution of the experiments (ca. 150 fs). The decay time of 0.32 ps is associated with the electron−phonon relaxation. This result is in line with data reported by Del Fatti et al.,[33] who measured electron−phonon relaxation times lower than 800 fs for silver nanoparticles of radio below 6 nm, as ours. The phonon−phonon coupling is on the order of several hundred picoseconds as measured for metallic nanoparticles in solution as well as in a glass matrix,[29] and thus the decay time of 203 ± 10 ps is assigned to this phenomenon. The decay times were found to be independent of the concentration of silver nanoparticles.

For the experiments performed with Rf and without Pec·AgNP, we must consider that the energy content of the S_1 state is 2.48 eV,[34] which means that our transient spectra shown in Figure 2b were obtained with an excess energy of 0.6 eV (λ^{exc} = 400 nm).

The EADS corresponding to the shortest time of 825 ± 41 fs shows negative $S_1 \leftarrow S_0$ signals (bleach) below ~560 nm, and $S_n \leftarrow S_1$ excited-state absorption (ESA) above this wavelength. This is in agreement with data obtained by Weigel et al.[33] who observed a biexponetial decay of similar spectra with lifetimes of 0.2 and 1.1 ps. These authors proposed that structural relaxation along low-frequency modes and solvent-controlled $^1\pi\pi^*\gamma \rightarrow {}^1n\pi^*$ conversion are behind the small spectral evolution on the subpicosecond time scale.

The slowest component of 4.7 ± 0.2 ns in Figure 2b, which also shows bleaching, and $S_1 \rightarrow S_0$ fluorescence in the form of stimulated emission (SE) regions is assigned to the (relaxed) $S_1 \rightarrow S_0$ decay[33] and is also in agreement with the fluorescence lifetime measured here and in the literature.[35] Under our experimental conditions this decay time also contains

DOI: 10.1021/acs.jpcc.6b06385
J. Phys. Chem. C 2016, 120, 21967−21975

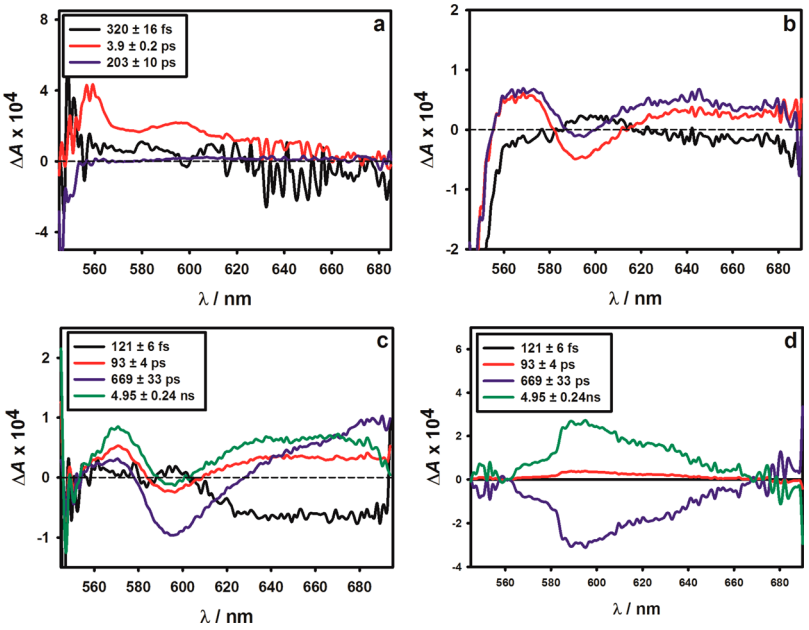

Figure 2. Comparison of transient spectra obtained in pump−probe experiments (λ^{exc} = 400 nm): (a) EADS of Pec·AgNP suspensions; (b) EADS of the Rf solution without Pec·AgNP; (c) EADS of the Rf solution in the presence of 1.8 μM Ag; (d) DADS corresponding to the EADS shown in panel (c).

information on any other species not decaying within the time window of the experiment (~5 ns), such as the triplet state ^{3}Rf* obtained by intersystem crossing from S_1. The other component, 21 ± 1 ps in our case and 100 ps in the paper by Weigel,[33] is visible over the full spectral window with very small amplitude. Weigel et al. proposed that the 100 ps component characterizes the signal decay in the ESA at 300 nm and bleach regions, suggesting that population is leaving the excited state to any other accessible state and returns to S_0.[33]

Figure 2c,d shows the EADS and DADS obtained with Rf in the presence of 1.8 μM Ag. Four components were necessary for the analysis of the signals. Figure 2c shows an EADS with a decay time of ca. 121 ± 6 fs, which is not present in the solution of Rf or in the suspensions of Pec·AgNP without Rf. This EADS does not arise from the S_1 excited state of Rf. However, since the decay time of 121 ± 6 fs is within the resolution time of the experiments (ca. 150 fs), the spectrum could have contributions of ultrafast phenomena such as coherent artifact,[36] and thus, no reliable information can be obtained from this EADS.

Comparison of the spectra of Figure 2a,b shows that the region of SE of Rf overlaps that of the shorter decay times of Pec·AgNP. Thus, we can speculate that the energy transfer from the complex to the nanoparticle plasmon would alter the electron distribution in the plasmon, which relaxes with the 93 ± 4 ps decay time (see Figure 2c,d for the EADS and DADS of this decay time).

The EADS with the two slower decay times of 669 ± 33 ps and 4.95 ± 0.24 ns look very similar (Figure 2c). The 669 ± 33 ps DADS mirrors the image of the 4.95 ± 0.24 ns DADS in the entire range from 540 to 700 nm (Figure 2d). This strongly suggests that the species with the 669 ± 33 ps decay time feeds the species with the 4.95 ± 0.24 ns decay time. The same argument in the analysis of DADS was used to support a sequential reaction in the tryptophan-to-heme electron transfer in ferrous myoglobins.[37] We propose that the excited state Rf···Pec·AgNP* with a lifetime of 669 ± 33 ps decays into a nondecaying state within our time window. The 4.95 ± 0.24 ns decay cannot be assigned to the lifetime of any state because it is within the upper edge of the time window of the experiment. Note that since the fraction of complexed Rf is only ~5% under the conditions of these experiments, the observation of the absorption of Rf···Pec·AgNP* requires a large molar absorption coefficient of the complex, probably due to a charge transfer interaction.

Laser Flash-Photolysis (λ^{exc} = 400 nm). All the experiments were performed under Ar-saturation. The spectra obtained in the absence and presence of Pec·AgNP could be well fitted with four components. Figure 3 shows the EADS of the fastest component (5.0 ns) for the sample without Pec·AgNP, which presents positive absorbance changes below 480 nm and negative changes of absorption above this wavelength. Thus, this component can be assigned to the S_1 state of Rf, which shows ESA below 480 nm and gives rise to the first

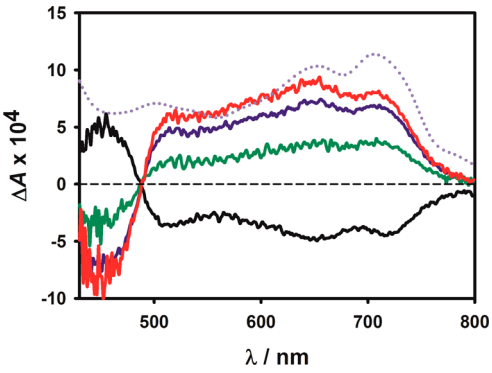

Figure 3. EADS obtained in laser flash-photolysis experiments ([Rf] = 53 μM) after 400 nm excitation for the first component (4.7 ns) in the absence of nanoparticles (black solid line) and in the presence of 0.87 μM Ag (green solid line), 2.2 μM Ag (blue solid line), and 4.4 μM Ag (red solid line). The literature triplet−triplet absorption spectrum of Rf is also shown (dotted line).[39]

DOI: 10.1021/acs.jpcc.6b06385
J. Phys. Chem. C 2016, 120, 21967−21975

excited triplet state ^{3}Rf* with absorption maximum at 710 nm.[38] For comparison, Figure 3 includes the literature absorption spectrum of the ^{3}Rf*.[39]

Since a constant value of 4.7 ns was obtained for the S_1 state of Rf in the TCSPC assays performed in the presence of Pec·AgNP, the shortest decay lifetime of the samples containing the nanoparticles was set to this value. In this fitting procedure, five components were needed. As can be seen in Figure 3, the EADS of the 4.7 ns component of Rf in the presence of particles looks very different from that obtained in their absence. The 4.7 ns EADS of Figure 3 have a main contribution of the triplet state of Rf, in agreement with the population of this state from the excited state of the Rf···Pec·AgNP* complex (see above). Thus, the absorption of the S_1 state of free Rf is masked by that of ^{3}Rf*, which has large absorption coefficients and longer lifetime. Note that below 480 nm bleaching is observed because the absorption of the triplet state is much lower than that of the ground state. Our data indicate that Rf···Pec·AgNP* decays to the triplet state of Rf (process 2 in Scheme 1). Because of the higher absorption coefficients of ^{3}Rf*, the decay of Rf···Pec·AgNP* to the fluorescent S_1 state of Rf cannot be neglected from these experiments. However, the fluorescence quenching shown in Figure S2 (see Supporting Information) does not support this decay route.

The second component is assigned to ^{3}Rf* (Figure 4a). The lifetime of this state 7.7 ± 0.7 μs is independent of the concentration of the nanoparticles. Again, bleaching below 480 nm is observed for the reasons given above.

Flash photolysis studies with solutions of Rf have shown the occurrence of reaction 6.

$$^3\mathrm{Rf}^* + \mathrm{SgRf}^{\bullet-} + \mathrm{S}^{\bullet+} \qquad (6)$$

where S is an electron donor.[39] This reaction occupies a prominent place in the photochemistry of Rf because many biologically significant molecules are capable of acting as electron donors.

The change of standard Gibbs energy $\Delta_{ET}G^\circ$ for the charge transfer reaction 6 involving ^{3}Rf* can be calculated from eq II, which includes the redox potential E° of the acceptor (^{3}Rf*) and the donor, and the triplet energy[40] of Rf, $\Delta E_{o,o}$ in J mol^{-1}. N_A is the Avogadro constant and e is the electron charge.

$$\Delta_{ET}G^\circ = N_A(eE^\circ(S^{\bullet+}/S) - eE^0(^3Rf/Rf^{\bullet-})) - \Delta E_{0,0} \qquad (II)$$

For calculations of $\Delta_{ET}G^\circ$, the reported values of E°(Rf/Rf$^{\bullet-}$) = −0.546 V vs NHE[41] and $\Delta E_{0,0}$ = 209 kJ mol^{-1}[34] will be used.

In particular, the ground state of Rf can act as a donor (reaction 3 in Scheme 1). In aqueous media at circumneutral pH Rf$^{\bullet-}$ is rapidly converted to the flavin semiquinone radical, RfH$^\bullet$ (reaction 5 in Scheme 1).[42] From the values of E° (Rf$^{\bullet+}$/Rf) = 2.28 V,[43] $\Delta_{ET}G^\circ$ = 63.3 kJmol^{-1} is obtained. For several reactions, low positive $\Delta_{ET}G^\circ$ values indicate the reversibility of the electron-transfer process.[44]

In order to verify whether the particles could also act as electron donors in reaction 6, $\Delta_{ET}G^\circ$ = −81.2 kJmol^{-1} was calculated from eq II taking the redox potential E°(Ag$^+$/Ag) ≈ 0.78 V[45] for silver nanoparticles of about 10 nm diameter. Thus, reaction (4) in Scheme 1 is feasible.

The lifetime of the third component in the absence of Pec·AgNP is 24.1 μs. In the presence of nanoparticles this lifetime, 18 ± 2 μs, is independent of the concentration of the nanoparticles. Two species contribute to this spectrum: the neutral HRf$^\bullet$ radical formed in reactions (3) and (4) after protonation of Rf$^{\bullet-}$ (reaction (5)) and the radical cation Rf$^{\bullet+}$ generated in reaction (3). The program is not able to separate the contributions of HRf$^\bullet$ and Rf$^{\bullet+}$ because of the overlapping of both absorption spectra. Figure 4b shows the EADS and the reported spectra for HRf$^\bullet$ and Rf$^{\bullet+}$. It can be clearly seen that the contribution of Rf$^{\bullet+}$ to the EADS is more relevant in the absence of nanoparticles, as expected from the competition between reactions (3) and (4).

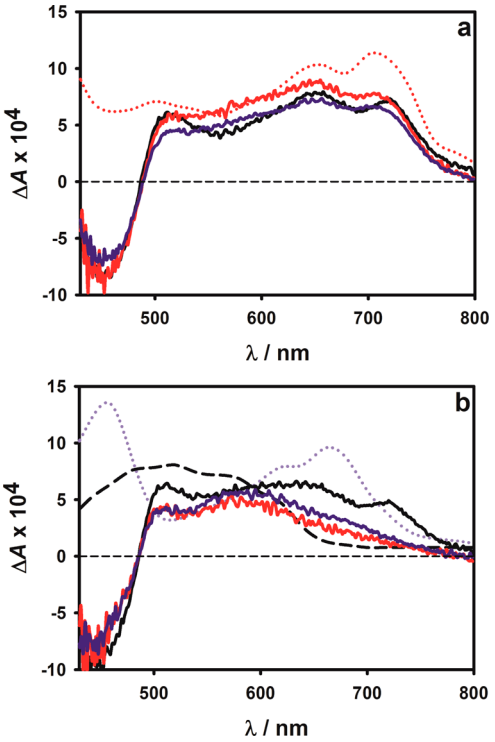

Figure 4. EADS obtained in laser flash-photolysis experiments ([Rf] = 53 μM) after 400 nm excitation: (a) the second component (7.7 μs) in the absence of nanoparticles (black solid line) and in the presence of 2.2 μM Ag (blue solid line) and 4.4 μM Ag (red solid line). The literature triplet−triplet absorption spectrum of Rf is also shown (dotted line).[35] (b) The third component (20 μs range) in the absence of nanoparticles (black solid line) and in the presence of 1.3 μM Ag (blue solid line) and 4.4 μM Ag (red solid line). The literature absorption spectra of the Rf$^+$ (dotted line) and HRf$^\bullet$ (dashed line) radicals.[39]

The fourth component with a lifetime of 530 ± 27 μs in the sample without nanoparticles and 257 ± 46 μs in the presence of Pec·AgNP is assigned to the HRf$^\bullet$ radical (either free or adsorbed) by comparison with the reported spectrum of this radical (see the EADS in Figure 5). It should be noted that these lifetimes are even longer than the time-window of the experiments, and thus, they cannot be accurately determined.

In the experiments performed with λ^{exc} = 400 nm in order to ensure that the absorbance of Pec·AgNP at the excitation wavelength is at least 10 times lower than that of Rf, the concentration of Ag was ≤4.4 μM. Thus, with the purpose of expanding the concentration range of Pec·AgNP we performed LFP experiments with λ^{exc} = 355 nm, where the absorption coefficient of the particles is lower than at 400 nm.

Laser Flash-Photolysis (λ^{exc} = 355 nm). LFP experiments (λ^{exc} = 355 nm) within a time window of 1−200 μs performed with Ar-saturated aqueous solutions of Rf showed formation of

DOI: 10.1021/acs.jpcc.6b06385
J. Phys. Chem. C 2016, 120, 21967−21975

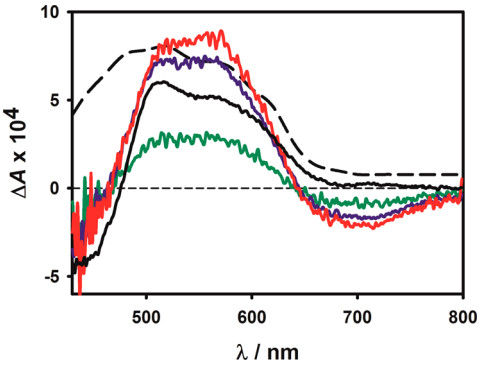

Figure 5. EADS of the fourth component (>100 μs) obtained in laser flash-photolysis experiments ([Rf] = 53 μM) after 400 nm excitation: in the absence of nanoparticles (black solid line) and in the presence of 0.87 μM Ag (green solid line), 2.2 μM Ag (blue solid line), and 4.4 μM Ag (red solid line). The literature absorption spectrum of $HRf^{\bullet}$ is also shown (dashed line).[39]

transient species. The absorption spectra taken at different times after the laser shot are shown in Figure 6.

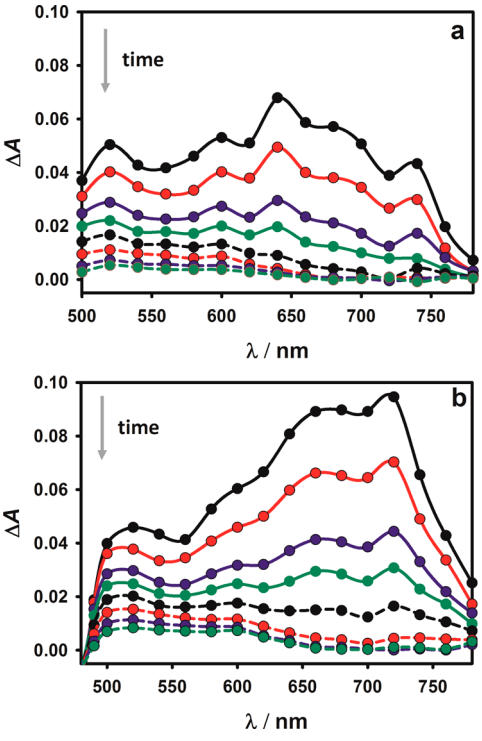

Figure 6. Absorbance spectra obtained from ns-LFP experiments (λ^{exc} = 355 nm) performed with Ar-saturated aqueous solutions of 57 μM Rf in the absence (a) and presence of 7.88 μM Ag (b) taken at different times after the laser shot: 2 μs (black solid line), 5 μs (red solid line), 10 μs (blue solid line), 15 μs (green solid line), 25 μs (black dashed line), 50 μs (red dashed line), 100 μs (blue dashed line), and 150 μs (green dashed line).

Comparison of the spectra in Figures 6a,b shows that the absorbance at the maximum of the triplet−triplet absorption spectrum (710 nm) is larger for the sample with nanoparticles, in agreement with the pump−probe and LFP assays performed at λ^{exc} = 400 nm. Since $^3Rf^*$, $RfH^{\bullet}$ and $Rf^{\bullet+}$ present overlapping absorption spectra and they all decay in the microsecond time scale, the global analysis was applied.

All the spectra could be well fitted with three components of lifetimes 8 ± 1, 35 ± 16, and 205 ± 31 μs (nondecaying spectra). All the results are in complete agreement with the LFP experiments performed with 400 nm excitation. Comparison of the DADS and kinetics of the species with shortest lifetime (Figure 7a) with that reported for $^3Rf^*$

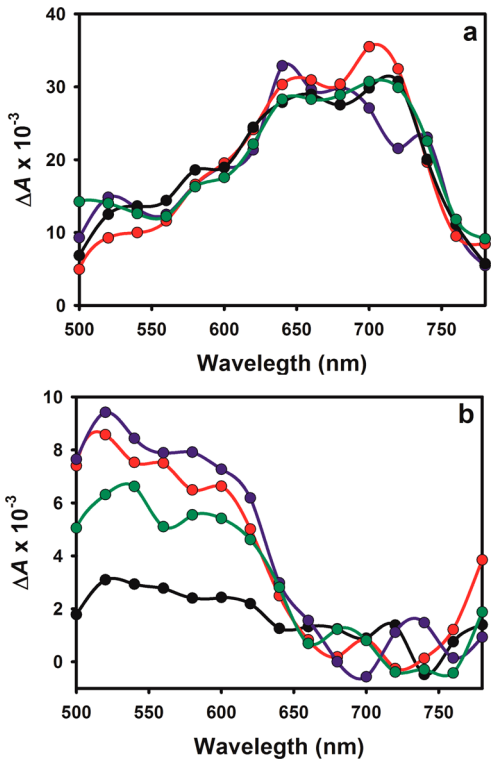

Figure 7. DADS corresponding to 8 ± 1 μs (a) and 205 ± 31 μs (b) obtained in laser flash-photolysis experiments ([Rf] = 57 μM) under Ar-saturation after 355 nm excitation in the absence (black) and presence of Ag: 1.18 μM (green), 1.57 μM (blue), 7.88 μM (red).

supports the assignment to this triplet state.[38,39] The exponential decay of $^3Rf^*$ is independent of the presence of increasing amounts of Pec·AgNP, also in line with the experiments with λ^{exc} = 400 nm. The component with the 35 ± 16 μs decay lifetime (DADS not shown) is formed through the decay of $^3Rf^*$ and presents contributions of both $HRf^{\bullet}$ and $Rf^{\bullet+}$, and the DADS of the third component is coincident with the reported absorption spectrum of $HRf^{\bullet}$ (see Figure 7b).[39]

In summary, excitation at 400 or 355 nm populates the singlet excited state of Rf ($^1Rf^*$) and the excited state of the Rf···Pec·AgNP* complex. The former has a lifetime of ca. 5 ns, whereas the latter has a shorter lifetime (ca. 700 ps). Intersystem crossing from $^1Rf^*$ or Rf···Pec·AgNP* to the triplet states free or Ag-bonded Rf ($^3Rf^*$) takes place (see Scheme 1). As a result, in the presence of the particles, population of the triplet state of Rf starts at shorter times and higher concentrations of $^3Rf^*$ are achieved.

In order to quantify the increase of the triplet yield of Rf in the presence of the nanoparticles, Figure 8a shows the plot of the ratio between the 710 nm absorbance change at t = 1 μs, ΔA^{710} in the presence of particles to that in the absence of particles, and ΔA_0^{710} obtained from LFP experiments at both excitation wavelengths (355 and 400 nm) vs the concentration of Ag. It can be seen in the figure that the increase of the triplet yield is independent of the excitation wavelength and that an

DOI: 10.1021/acs.jpcc.6b06385
J. Phys. Chem. C 2016, 120, 21967−21975

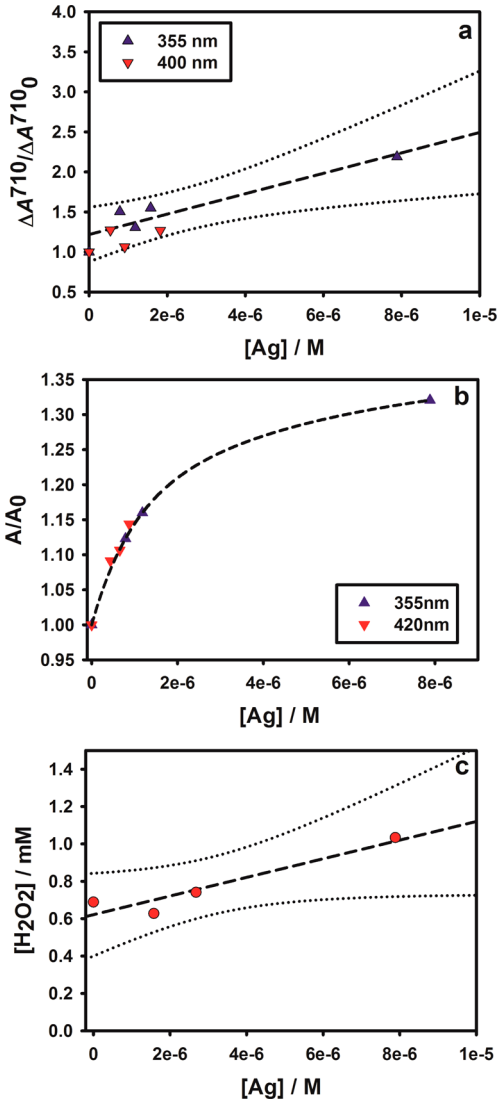

Figure 8. (a) Plot of $\Delta A^{710}/\Delta A_0{}^{710}$ vs [Ag]. (b) Plot of the ratio of the areas (A/A_o) of the singlet oxygen phosphorescence signals vs [Ag]. (c) Plot of [H_2O_2] vs [Ag].

increase of ca. 100% in the triplet yield of Rf is achieved in the presence of the highest concentration of the nanoparticles.

Under aerobic conditions the energy transfer from ^{3}Rf* to ground state oxygen ($^3O_2$) takes place to yield $O_2(^1\Delta_g)$ (reaction (7) in Scheme 2). From the increase in the triplet yield in the presence of the nanoparticles, a concomitant enhancement of the $O_2(^1\Delta_g)$ yield is expected, as can be seen in Figure 8b, which shows the plot of the ratio of the fluence and

Scheme 2. Formation of $^1O_2$ and $O_2^{\bullet-}$ Under Aerobic Conditions

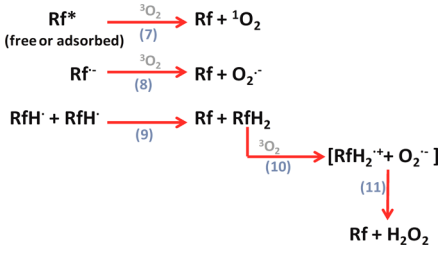

absorbance normalized areas of the time-resolved $O_2(^1\Delta_g)$ phosphorescence in the presence (A) and absence of the nanoparticles (A_o) vs [Ag]. This result is in agreement with data obtained by indirect methods.[14] Note that only an increase of ca. 30% in the amount of singlet oxygen is achieved for the highest concentration of nanoparticles.

Rf produces $O_2^{\bullet-}$ with a quantum yield Φ_{H2O2} = 0.009.[46] A higher amount of ^{3}Rf* formed in the presence of Pec·AgNP is also expected to result in a higher yield of $O_2^{\bullet-}$ (reaction (8)), which generates H_2O_2 by disproportionation. Additionally, other processes reported in the literature indicate a further contribution to the observed enhancement of hydrogen peroxide in the presence of Pec·AgNP (Figure 8c). In fact, the bimolecular decay of RfH$^\bullet$ yields equimolar amounts of Rf and fully reduced Rf (RfH_2) (process (9) in Scheme 2), which under aerobic conditions is oxidized to the $RfH_2^{\bullet+}$ radical and $O_2^{\bullet-}$ and finally Rf and H_2O_2 (reactions (10) and (11)).[47] The 60% measured enhancement in the concentration of hydrogen peroxide production for the samples with the highest concentration of nanoparticles should be considered as a lower limit because silver nanoparticles are known to catalyze the decomposition of hydrogen peroxide.[48]

From the LFP experiments we have no evidence for a shortening of the lifetime of ^{3}Rf* (ca. 8 μs at both excitation wavelengths) in the presence of the nanoparticles. This can be due to the limited concentration range of Pec·AgNP employed in the experiments to preclude light absorption by the nanoparticles and to the fact that the rate of reaction (3) is greater than that of reaction (4), i.e., $k_3 \times [Rf] \geq k_4 \times [Ag]$. The reported value of k_3 is 6×10^8 M^{-1} s^{-1},[49] [Rf] = 53 μM, and [Ag] is $\leq$4.4 μM. For the collisional encounter between free ^{3}Rf* and the nanoparticles, the diffusion-controlled rate constant estimated by the Smoluchowski equation is 2.7×10^7 M^{-1} s^{-1}[50] (see Supporting Information), and thus, $k_3 \times [Rf] \geq k_4 \times [Ag]$. The electron transfer from Ag atoms of the particle and adsorbed ^{3}Rf* is not diffusion-controlled, and it is thus expected to be faster. However, this process is not reflected in the overall decay rate of ^{3}Rf* because the amount of adsorbed Rf is $\leq$5% in the LFP experiments with λ^{exc} = 400 nm, and $\leq$14% in the experiments with λ^{exc} = 355 nm.

However, evidence for a higher amount of Rf^+ in the samples without the particles is presented in Figure 7b.

CONCLUSIONS

The excited state of the riboflavin–Ag complex feeds the triplet state of the sensitizer, which results in an enhanced intersystem crossing process in the presence of the nanoparticles. The higher amounts of riboflavin triplet states formed result in higher yields of singlet oxygen and superoxide radical anion generation, as evaluated from the concentration of hydrogen peroxide produced in the irradiated colloidal suspensions. The enhancement in the production of hydrogen peroxide ($\geq$60% for samples containing 8 μM Ag) is larger than that observed in the production of singlet oxygen due to electron transfer from the silver nanoparticles to riboflavin triplet states. As a result, the effect on singlet oxygen should contribute to a better performance of riboflavin as a sensitizer applied to the photodynamic therapy of tumors.

ASSOCIATED CONTENT

Supporting Information

The Supporting Information is available free of charge on the ACS Publications website at DOI: 10.1021/acs.jpcc.6b06385.

DOI: 10.1021/acs.jpcc.6b06385
J. Phys. Chem. C 2016, 120, 21967–21975

Size distribution histogram of Pec·AgNP. TEM image of Pec·AgNP. UV−vis absorption, extinction, and scattering spectra of a 11.7 μM suspension of Pec·AgNP. Zeta potential measurements of Pec·AgNP as a function of pH. FTIR spectra of pectin and Pec·AgNP. Fluorescence lifetimes of Rf in the absence and presence of Pec·AgNP. Emission spectra of Rf in the absence and presence of Pec·AgNP. Calculation of the diffusion-controlled rate constant with the Smoluchowski equation (PDF)

AUTHOR INFORMATION

Corresponding Author

*Tel: +54 221 4257430. Fax: +54 221 4254642. E-mail: dmartire@inifta.unlp.edu.ar.

Notes

The authors declare no competing financial interest.

ACKNOWLEDGMENTS

This work has been supported by grant PICT 2012-1817 from ANPCyT, Argentina. We want to thank Prof. Ana Moore for providing laboratory facilities at ASU and the U.S. Department of Energy, Office of Science, Office of Basic Energy Sciences, under Award Number DESC0001016 for funding. We also thank Prof. Peter Ogilby, Michael Westberg Sørensen, and Mikkel Bregnhøj from the University of Aarhus for the singlet oxygen measurements at the excitation wavelength of 420 nm. M.B.R.A. and J.J.R. thank CONICET for a graduate studentship. S.G.B. and M.C.G. are research members of CONICET, Argentina. D.O.M. is a research member of CIC, Buenos Aires, Argentina.

REFERENCES

(1) Foote, C. S.; Clennan, E. L. *Active Oxygen in Chemistry*; Foote, C. S., Valentine, J. S., Greenberg, A., Liebman, J. F., Eds.; Chapman and Hall: London, 1995.

(2) Schweitzer, C.; Schmidt, R. Physical Mechanisms of Generation and Deactivation of Singlet Oxygen. *Chem. Rev.* **2003**, *103*, 1685−1757.

(3) Paterson, M. J.; Christiansen, O.; Jensen, F.; Ogilby, P. R. Invited review - Overview of Theoretical and Computational Methods Applied to the Oxygen-Organic Molecule Photosystem. *Photochem. Photobiol.* **2006**, *82*, 1136−1160.

(4) Bonnett, R. *Chemical Aspects of Photodynamic Therapy*; Gordon and Breach Science Publishers: Amsterdam, 2000.

(5) Wilkinson, F.; Helman, W. P.; Ross, A. B. J. Quantum Yields for the Photosensitized Formation of the Lowest Electronically Excited Singlet State of Molecular Oxygen in Solution. *J. Phys. Chem. Ref. Data* **1993**, *22*, 113−275.

(6) Planas, O.; Macia, N.; Agut, M.; Nonell, S.; Heyne, B. Distance-Dependent Plasmon-Enhanced Singlet Oxygen Production and Emission for Bacterial Inactivation. *J. Am. Chem. Soc.* **2016**, *138*, 2762−2768.

(7) Kreibig, U.; Vollmer, M. *Optical Properties of Metal Clusters*; Springer: Berlin, 1995.

(8) Wiederrecht, G. P.; Wurtz, G. A.; Bouhelier, A. Ultrafast Hybrid Plasmonics. *Chem. Phys. Lett.* **2008**, *461*, 171−179.

(9) Murphy, S.; Huang, L.; Kamat, P. V. Charge-Transfer Complexation and Excited-State Interactions in Porphyrin-Silver Nanoparticle Hybrid Structures. *J. Phys. Chem. C* **2011**, *115*, 22761−22769.

(10) Cardoso, D. R.; Libardi, S. H.; Skibsted, L. H. Riboflavin as a Photosensitizer. Effects on human health and food quality. *Food Funct.* **2012**, *3*, 487.

(11) Baier, J.; Maisch, T.; Maier, M.; Engel, E.; Landthaler, M.; Bäumler, W. Singlet Oxygen Generation by UVA Light Exposure of Endogenous Photosensitizers. *Biophys. J.* **2006**, *91*, 1452−1459.

(12) García, N.; Criado, S.; Massad, W. Riboflavin as a Visible-Light-Sensitiser in the Aerobic Photodegradation of Ophthalmic and Sympathomimetic Drugs. In *Flavins: Photochemistry and Photobiology*; Comprehensive Series in Photosciences; Silva, E., Edwards, A. M., Eds; RSC: London, 2006.

(13) Ferrari, G. V.; Natera, J.; Montaña, M. P.; Muñoz, V.; Gutiérrez, E. L.; Massad, W.; Miskoski, S.; García, N. A. Scavenging of Photogenerated ROS by Oxicams. Possible Biological and Environmental Implications. *J. Photochem. Photobiol., B* **2015**, *153*, 233−239.

(14) de Melo, L. S.; Gomes, A. S.; Saska, S.; Nigoghossian, K.; Messaddeq, Y.; Ribeiro, S. J. L.; de Araujo, R. E. Singlet Oxygen Generation Enhanced by Silver-Pectin Nanoparticles. *J. Fluoresc.* **2012**, *22*, 1633−1638.

(15) Balachandran, Y. L.; Girija, S.; Selvakumar, R.; Tongpim, S.; Gutleb, A. C.; Suriyanarayanan, S. Differently Environment Stable Bio-Silver Nanoparticles: Study on their Optical Enhancing and Antibacterial Properties. *PLoS One* **2013**, *8*, e77043.

(16) Liu, X.; Atwater, M.; Wang, J.; Huo, Q. Extinction Coefficient of Gold Nanoparticles with Different Sizes and Different Capping Ligands. *Colloids Surf., B* **2007**, *58*, 3−7.

(17) Petushkov, V. N.; van Stokkum, I. H. M.; Gobets, B.; van Mourik, F.; Lee, J.; van Grondelle, R.; Visser, A. J. W. G. Ultrafast Fluorescence Relaxation Spectroscopy of 6,7-Dimethyl-(8-ribityl)-lumazine and Riboflavin, Free and Bound to Antenna Proteins from Bioluminescent Bacteria. *J. Phys. Chem. B* **2003**, *107*, 10934−10939.

(18) Bertolotti, S. G.; Previtali, C. M. The Excited States Quenching of Safranine T by p-Benzoquinones in Polar Solvents. *J. Photochem. Photobiol., A* **1997**, *103*, 115−119.

(19) Llansola-Portoles, M. J.; Bergkamp, J. J.; Tomlin, J.; Moore, T. A.; Kodis, G.; Moore, A. L.; Cosa, G.; Palacios, R. E. Photoinduced Electron Transfer in Perylene-TiO_2 Nanoassemblies. *Photochem. Photobiol.* **2013**, *89*, 1375−1382.

(20) van Stokkum, I. H. M.; Larsen, D. S.; van Grondelle, R. Global and Target Analysis of Time-Resolved Spectra. *Biochim. Biophys. Acta, Bioenerg.* **2004**, *1657*, 82−104.

(21) Carlos, L.; Pedersen, B. W.; Ogilby, P. R.; Mártire, D. O. The Role of Humic Acid Aggregation on the Kinetics of Photosensitized Singlet Oxygen Production and Decay. *Photochem. Photobiol. Sci.* **2011**, *10*, 1080−1086.

(22) Ogilby, P. R. Singlet Oxygen: There is Indeed Something New Under the Sun. *Chem. Soc. Rev.* **2010**, *39*, 3181−3209.

(23) Allain, C. C.; Poon, L. S.; Chan, C. S. G.; Richmond, W.; Fu, P.C. Enzymatic Determination of Total Serum Cholesterol. *E. Clin. Chem.* **1974**, *20*, 470−475.

(24) Merga, G.; Wilson, R.; Lynn, G.; Milosavljevic, B. H.; Meisel, D. Redox Catalysis on "Naked" Silver Nanoparticles. *J. Phys. Chem. C* **2007**, *111*, 12220−12226.

(25) Shamolina, I. I.; Bochek, A. M.; Zabivalova, N. M.; Medvedeva, D. A.; Grishanov, S. A. An Investigation of Structural Changes in Short Flax Fibres in Chemical Treatment. *Fibres Text. East Eur.* **2003**, *11*, 33−36.

(26) Gnanasambandam, R.; Proctor, A. Determination of Pectin Degree of Esterification by Diffuse Reflectance Fourier Transform Infrared Spectroscopy. *Food Chem.* **2000**, *68*, 327−332.

(27) Benesi, H. A.; Hildebrand, J. H. A Spectrophotometric Investigation of the Interaction of Iodine with Aromatic Hydrocarbons. *J. Am. Chem. Soc.* **1949**, *71*, 2703−2707.

(28) Mokashi, V. V.; Walekar, L. S.; Anbhule, P. V.; Lee, S. H.; Patil, S. R.; Kolekar, G. B. Study of Energy Transfer Between Riboflavin (Vitamin B2) and AgNPs. *J. Nanopart. Res.* **2014**, *16*, 2291.

(29) Link, S.; El-Sayed, M. A. Optical Properties and Ultrafast Dynamics of Metallic Nanocrystals. *Annu. Rev. Phys. Chem.* **2003**, *54*, 331−366.

(30) Link, S.; El-Sayed, M. A. Spectral Properties and Relaxation Dynamics of Surface Plasmon Electronic Oscillations in Gold and

DOI: 10.1021/acs.jpcc.6b06385
J. Phys. Chem. C 2016, 120, 21967−21975

Silver Nanodots and Nanorods. *J. Phys. Chem. B* **1999**, *103*, 8410−8426.
(31) Ahmadi, T. S.; Logunov, S. L.; El-Sayed, M. A. Picosecond Dynamics of Colloidal Gold Nanoparticles. *J. Phys. Chem.* **1996**, *100*, 8053−8056.
(32) Link, S.; Burda, C.; Wang, Z. L.; El-Sayed, M. A. Electron Dynamics in Gold and Gold−Silver Alloy Nanoparticles: The Influence of a Nonequilibrium Electron Distribution and the Size Dependence of the Electron−Phonon Relaxation. *J. Chem. Phys.* **1999**, *111*, 1255−1264.
(33) Weigel, A.; Dobryakov, A. L.; Veiga, M.; Pérez Lustres, J. L. Photoinduced Processes in Riboflavin: Superposition of $\pi\pi^*$- $n\pi^*$ States by Vibronic Coupling, Transfer of Vibrational Coherence, and Population Dynamics Under Solvent Control. *J. Phys. Chem. A* **2008**, *112*, 12054−12065.
(34) Porcal, G.; Bertolotti, S. G.; Previtali, C. M.; Encinas, M. V. Electron Transfer Quenching of Singlet and Triplet Excited States of Flavins and Lumichrome by Aromatic and Aliphatic Electron Donors. *Phys. Chem. Chem. Phys.* **2003**, *5*, 4123−4128.
(35) Arce, V. B.; Scotto, J.; Allegretti, P. E.; Melo, M. A., Jr.; Airoldi, C.; Salum, M. L.; Erra-Balsells, R.; Pis Diez, R.; Mártire, D. O. A Combined Experimental and Computational Investigation of the Fluorescence Quenching of Riboflavin by Cinnamic Alcohol Chemisorbed on Silica Nanoparticles. *J. Phys. Chem. C* **2014**, *118*, 15348−15355.
(36) Lebedev, M. V.; Misochko, O. V.; Dekorsy, T.; Georgiev, N. On the Nature of "Coherent Artifact. *J. Exp. Theor. Phys.* **2005**, *100*, 272−282.
(37) Monni, R.; Al Haddad, A.; van Mourik, F.; Auböck, G.; Chergui, M. Tryptophan-to-Heme Electron Transfer in Ferrous Myoglobins. *Proc. Natl. Acad. Sci. U. S. A.* **2012**, *112*, 5602−5606.
(38) Orellana, B.; Rufs, A. M.; Encinas, M. V.; Previtali, C. M.; Bertolotti, S. The Photoinitiation Mechanism of Vinyl Polymerization by Riboflavin/Triethanolamine in Aqueous Medium. *Macromolecules* **1999**, *32*, 6570−6573.
(39) Li, H.; Melø, T. B.; Razi Naqvi, K. Triplets, Radical Cations and Neutral Semiquinone Radicals of Lumiflavin and Riboflavin: An Overhaul of Previous Pump−Probe Data and New Multichannel Absolute Absorption Spectra. *J. Photochem. Photobiol., B* **2012**, *106*, 34−39.
(40) Braslavsky, S. E. Glossary of Terms Used in Photochemistry 3rd Edition. *Pure Appl. Chem.* **2007**, *79*, 293−465.
(41) Tan, S. L. J.; Webster, R. D. Electrochemically Induced Chemically Reversible Proton-Coupled Electron Transfer Reactions of Riboflavin (Vitamin B2). *J. Am. Chem. Soc.* **2012**, *134*, 5954−5964.
(42) Lu, C.; Bucher, G.; Sander, W. Photoinduced Interactions Between Oxidized and Reduced Lipoic Acid and Riboflavin (Vitamin B2). *ChemPhysChem* **2004**, *5*, 47−56.
(43) Kishore, K.; Moorthy, P. N.; Guha, S. N. Pulse Radiolysis Study of One Electron Oxidation of Riboflavin. *Int. J. Radiat. Appl. Instrum. C. Radiat. Phys. Chem.* **1991**, *38*, 119−125.
(44) Arce, V.; Bertolotti, S.; Oliveira, F.; Airoldi, C.; Gonzalez, M. C.; Allegretti, P. E.; Mártire, D. O. Safranine-T Triplet-State Quenching by Modified Silica Nanoparticles. *J. Phys. Chem. C* **2011**, *115*, 18122−18130.
(45) Ivanova, O. S.; Zamborini, F. P. Size-Dependent Electrochemical Oxidation of Silver Nanoparticles. *J. Am. Chem. Soc.* **2010**, *132*, 70−72.
(46) Krishna, C. M.; Uppuluri, S.; Riesz, P.; Zigler, J. S.; Balasubramanian, D. A study on the Photolysis Efficiencies of Some Lens Constituents. *Photochem. Photobiol.* **1991**, *54*, 51−58.
(47) Criado, S.; García, N. A. A Comparative Kinetic and Mechanistic Study Between Tetrahydrozoline and Naphazoline Toward Photogenerated Reactive Oxygen Species. *Photochem. Photobiol.* **2010**, *86*, 23−30.
(48) He, D.; Jones, A. M.; Garg, S.; Pham, A. N.; Waite, T. D. Silver Nanoparticle−Reactive Oxygen Species Interactions: Application of a Charging−Discharging Model. *J. Phys. Chem. C* **2011**, *115*, 5461−5468.
(49) Lu, C.; Han, Z.; Liu, G.; Cai, X.; Chen, Y.; Yao, S. Photophysical and Photochemical Processes of Riboflavin (Vitamin B2) by Means of the Transient Absorption Spectra in Aqueous Solution. *Sci. China, Ser. B: Chem.* **2001**, *44*, 39−48.
(50) Shield, S. R.; Harris, J. M. Reaction Kinetics at Dispersed-Colloid/Solution Interfaces: Benzophenone Triplet-State Quenching by Methylated Silica Particles. *J. Phys. Chem. B* **2000**, *104*, 8527−8535.

DOI: 10.1021/acs.jpcc.6b06385
J. Phys. Chem. C 2016, 120, 21967−21975